

Hybridization of an s -wave impurity with graphene lattice

Hoa T. M. Nghiem¹, Tien-Lam Pham^{1,2}, Ngoc-Linh Nguyen^{3,4}, and Hung T. Dang^{1,3,†}

¹*Phenikaa Institute for Advanced Study, Phenikaa University, Yen Nghia, Ha Dong district, Hanoi 12116, Vietnam*

²*Faculty of Computer Science, Phenikaa University, Yen Nghia, Ha Dong district, Hanoi 12116, Vietnam*

³*Faculty of Materials Science and Engineering, Phenikaa University, Yen Nghia, Ha Dong district, Hanoi 12116, Vietnam*

⁴*PHENIKAA Research and Technology Institute (PRATI), A&A Green Phoenix Group JSC, No. 167 Hoang Ngan, Trung Hoa, Cau Giay, Hanoi 11313, Vietnam*

E-mail: †hung.dangthe@phenikaa-uni.edu.vn

Received July 8, 2024

Accepted for publication (Editor will insert the date when the article is accepted)

Published (Editor will insert the date when the article is published)

Abstract. *Hybridization function is a quantity characterizing electron hopping between an impurity and a host material in which the impurity resides, a full understanding of it is crucial for studying correlation effects in various impurity problems. This work studies the hybridization function for the Anderson impurity model describing a single-orbital impurity on a honeycomb lattice simulating graphene and presents a calculation approach to obtain this function at low energy. Within this approach, the general form of the hybridization function in graphene is presented and analytical expressions of low-energy hybridization spectrum are obtained. The results quantitatively match numerical solutions for different impurity positions on the lattice. The effect of the low-energy hybridization spectrum and the capability to predict the correlated effects of the impurity problem are discussed thoroughly, suggesting that different types of pseudogap Kondo effect may occur at different impurity positions.*

Keywords: Anderson impurity model, pseudogap Kondo effect, hybridization function, honeycomb lattice, graphene.

Classification numbers: 73.22.Pr, 72.15.Qm, 71.27.+a.

1. Introduction

Since its first synthesis twenty years ago [1, 2], graphene has always been the most investigated material thanks to its exotic electronic and mechanical properties, in particular the Dirac fermion characteristic around the Fermi level [3, 4]. These unique properties also make graphene an optimal host lattice for a wide variety of adatoms [5, 6], which may lead to potential applications such as electronic devices [7], single-ion magnets [8], single-atom catalysts [9], or tuning the electronic properties by doping [10], etc. To step closer to the realization of those applications, it is crucial to understand the behaviors of impurities on graphene. Typical research focuses on electronic structures and crystal structures of the impurities on graphene, such as to determine the defect states or impurity positions in stable states [5, 6, 11, 12]. However, when a magnetic adatom (such as a transition metal or a rare-earth atom) is adsorbed on graphene, electron correlation effect is significant, leading to more intriguing phenomena. One of the fundamental issues is the Kondo effect of a magnetic adatom on graphene [13–16]. It is a correlation effect that is originated from the Coulomb interaction between electrons in the adatom. Normally, for a magnetic adatom on metallic surface, conduction electrons from the surface cause a screening effect to the magnetic moment of the adatom, thus when the temperature is below a specific energy scale (the Kondo temperature), the magnetic local moment of the adatom is completely screened [17]. However, graphene is a special semimetal with linear energy dispersion around the Fermi level and the density of states (DOS) vanishing exactly at the charge neutral point. Therefore, graphene is a potential candidate for the realization of the so-called “pseudogap” Kondo models, a special class of Kondo models proposed in the 1990s [18–20].

Pseudogap Kondo problem can be described using the Kondo model or, more generally, the Anderson impurity model [20]. In this model, the DOS of the host material $\nu(\omega)$ exhibits semimetal characteristic. It vanishes at zero frequency and increases as a power law of frequency $\nu(\omega) \sim |\omega|^r$. Thus, pseudogap Kondo problems are classified by the parameter r [20]. Unlike conventional Kondo problems, the Kondo screening phase in the pseudogap Kondo problem does not always exist. Depending on r , one can tune the system parameters such as the impurity energy level or the correlation strength in order to switch on the Kondo screening effect, thus observing a quantum phase transition in the system [20–22]. Consequently, for different values of r , the phase diagram of the pseudogap Kondo model and the nature of the quantum critical point changes accordingly.

In this work, we focus on the problem of a single-orbital impurity placed on a graphene sheet. We study the Anderson impurity model [23] with a honeycomb lattice as the host material, simulating the graphene sheet. We consider the low-energy noninteracting physics of the model depending on the position of the impurity on the lattice and attempt to obtain analytic formulas characterizing the hybridization between the impurity and the lattice around the Fermi level. We also emphasize that this work does not fully treat the correlation effects but focuses on the noninteracting aspect of the model.

The structure of the paper is as follows: Sec. 2 describes the model and introduces the hybridization function, which is the main focus in this work. The general form of the hybridization between the impurity and the host material is presented Sec. 3. Sec. 4 presents detailed calculations for this hybridization at low energy and shows the analytic results in comparison with numerical ones. Finally, Sec. 5 concludes our work.

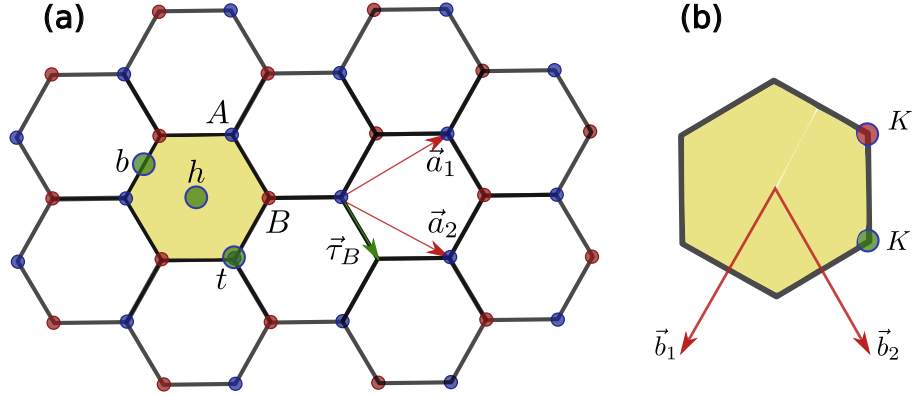


Fig. 1. (a) The honeycomb lattice (graphene) with two sublattices A (red circles) and B (blue circles) with impurities (green circles) at the bridge site b , at the hollow site h and at the top site t . The distance between two nearest neighbor site of the lattice is set to 1. Two primitive vectors are $a_1 = (3/2, \sqrt{3}/2)$ and $a_2 = (3/2, -\sqrt{3}/2)$. $\tau_B = (1/2, -\sqrt{3}/2)$ is the position vector of a B site in a unit cell, $\tau_A = (0, 0)$ for the corresponding A site is not shown. (b) The first Brillouin zone (BZ1) of the honeycomb lattice in panel (a) (yellow region). $b_1 = (-2\pi/3, -2\pi/\sqrt{3})$ and $b_2 = (2\pi/3, -2\pi/\sqrt{3})$ are two basis vectors of the reciprocal space. $K = (2\pi/3, 2\pi/(3\sqrt{3}))$ and $K' = (2\pi/3, -2\pi/(3\sqrt{3}))$ are the positions of two valleys.

2. Formalism

2.1. Model

In this work, we focus on the Anderson impurity model [23], which is a fundamental model to describe magnetic impurity on a lattice and fully contains the single-channel Kondo physics. Specifically, our impurity problem is simplified as an s -wave single-orbital impurity placed on a graphene sheet. In this model, conduction electrons of the host material (graphene) are assumed noninteracting, while impurity electrons are correlated, as described by the onsite Hubbard interaction. The Hamiltonian has three parts: (1) H_{latt} describing the hoppings of conduction electrons on the lattice of the host material, (2) H_{imp} describing the impurity electrons, and (3) H_{hyb} characterizing the hybridization between the host material and the impurity.

$$H = H_{latt} + H_{imp} + H_{hyb}. \quad (1)$$

Graphene, the host material, is a two-dimensional semimetal which can be well-described by a honeycomb lattice as illustrated in Figure 1(a). At the charge neutral state, each site of the graphene sheet has a valence electron of p_z orbital, which can be assumed as a single-orbital site containing only one electron on average. These electrons are conductive, noninteracting, and can hop between lattice sites. Thus, the lattice Hamiltonian H_{latt} has a quadratic form characterizing the kinetic energy of these electrons, of which the general form reads

$$H_{latt} = \sum_{k\alpha\beta\sigma} c_{k\alpha\sigma}^\dagger h_{\alpha\beta}(k) c_{k\beta\sigma} - \sum_{k\alpha\sigma} \mu c_{k\alpha\sigma}^\dagger c_{k\alpha\sigma}, \quad (2)$$

where $c_{k\alpha\sigma}^\dagger$ ($c_{k\alpha\sigma}$) is the creation (annihilation) operator for electron of spin σ , k is the vector in the first Brillouin zone (BZ1) of the honeycomb lattice [see Fig. 1(b)], α and β are the sublattice indices, and μ is the chemical potential. $\hat{h}(k)$ is a 2×2 k -dependent hopping matrix, describing all possible kinds of electron hopping in the lattice. To construct $\hat{h}(k)$ matrix, one employs the tight-binding approach, which considers only electron hoppings between sites in short distances such as the nearest-neighbor hopping (t), the next nearest-neighbor hopping (t'), etc. As we focus on the low energy region around the Fermi level, the nearest neighbor hopping t is the dominant term. Thus for simplicity, we only keep t in our calculations (which will be used as the basic energy scale) and neglect hoppings to sites further than the nearest ones. Then the tight-binding form of $\hat{h}(k)$ is [24]

$$\hat{h}(k) = \begin{pmatrix} 0 & \pi_k \\ \pi_k^* & 0 \end{pmatrix} \quad (3)$$

where

$$\pi_k = -te^{ik \cdot \tau_B} \left(1 + e^{-ik \cdot a_2} + e^{-ik \cdot (a_1 - a_2)} \right). \quad (4)$$

With only the hopping t , in order for the graphene lattice at the charge neutral point, a requirement to observe the pseudogap Kondo physics [20], the chemical potential must vanish. Consequently, we keep $\mu = 0$ throughout this work.

The local Hamiltonian of the impurity H_{imp} for the Kondo problem normally contains terms characterizing the correlation in the impurity [25]. For the single-orbital s -wave impurity, H_{imp} is composed of the well-known Hubbard interaction $Un_\uparrow n_\downarrow$ (where U is the interaction strength, n_σ is the impurity electron occupancy operator) and a term corresponding to the impurity energy level ϵ_d . However, as we do not fully treat the correlation effects originated from the impurity, H_{imp} is not considered in this work.

The hybridization Hamiltonian is the part that describes the hoppings of electrons between the impurity and the host material

$$H_{hyb} = \sum_{k,\alpha,\sigma} \left(V_{k\alpha} c_{\alpha k \sigma}^\dagger d_\sigma + V_{k\alpha}^* d_\sigma^\dagger c_{\alpha k \sigma} \right), \quad (5)$$

where d_σ^\dagger (d_σ) is the creation (annihilation) operator of impurity electrons, $V_{k\alpha}$ is the hybridization strength presented in the k -space.

2.2. Hybridization function

The hybridization function $\Delta(z)$ is the main object in this study. It is a quantity characterizing dynamically the connection between the impurity and the host material (the graphene sheet), which mostly occurs in the context of dynamical mean-field theory [26]. Normally it is represented in the frequency domain, thus we use a generalized frequency z as the variable for the function. $\Delta(z)$ is the remaining term attached with $V_{k\alpha}$ after integrating out all creation and annihilation operators of conduction electrons $c_{\alpha k \sigma}^\dagger, c_{\alpha k \sigma}$ [17, 26, 27]. For the case of the honeycomb lattice in this work, the form of the hybridization function is

$$\Delta(z) = \sum_{k\alpha\beta} V_{k\alpha}^* \left[(\mathbb{1}z - \hat{h}(k))^{-1} \right]_{\alpha\beta} V_{k\beta}. \quad (6)$$

The hybridization function enters the formula of the impurity one-particle Green function as [26]

$$G_{\sigma}(z) = \frac{1}{z - \epsilon_d - \Delta(z) - \Sigma_{\sigma}(z)}. \quad (7)$$

$\Sigma_{\sigma}(z)$ is the impurity self-energy representing the correlation effect at the impurity, which depends strongly on the interaction strength (the Hubbard coefficient U in this case, the Anderson impurity model) and vanishes when there is no interaction. There are various complicated methods to treat the correlation effect and obtain the self-energy [26, 28]. However, understanding $\Delta(z)$ provides a qualitative perspective of the final results even without further calculations for the correlation effect. Moreover, graphene, as a special two-dimensional material, might result in novel characteristics of the hybridization. Therefore, the hybridization function is under investigation in this study.

We also note that the generalized frequency z used in Eq. (7) allows for deriving different forms of the Green function. If replacing z by the Matsubara frequency $i\omega_n = (2n + 1)\pi/\beta$, one obtains the Matsubara Green function (which is useful when deploying stochastic methods such as Quantum Monte Carlo [28]); if replacing z by $\omega + i0^+$ ($\omega - i0^-$), one obtains the retarded (advanced) Green function, from which the spectral function is directly derived [29].

3. General form of $\Delta(z)$

In conventional pseudogap Anderson impurity model, the pseudogap feature is often described based on the DOS of the host material [20], which has the form $\nu(\omega) \sim |\omega|^r$, whereas the “pseudogap” feature that the impurity awares of comes directly from the hybridization function. However, in conventional model, the DOS has a theoretical form $\nu \sim |\omega|^r$, the hybridization spectrum $h(\omega) = -\frac{1}{\pi}\text{Im}\Delta(\omega + i0^+)$ is only different from the DOS by a prefactor, thus it is acceptable to consider only the DOS when treating the pseudogap feature. In realistic calculations, when treating the host material as a lattice, the hybridization spectrum can be strongly different from the DOS depending on where the impurity is located on the lattice.

The honeycomb lattice simulating graphene exhibits linear DOS around the charge neutral point [4]. From our previous work [24], the hybridization function can be significantly modified depending on the position of the impurity on the lattice. However, detailed calculations for these results have not been given. This work will present our full derivation for the analytic forms of $\Delta(\omega)$ at low frequency and discuss the physics implied from these results.

We focus on the three most common positions of impurity on graphene lattice [16]: (1) on top of an atom (at the top site t), (2) at the bridge site b , and (3) at the hollow site h [depicted in Figure 1(a)]. First, we assume that

$$V_{k\alpha} = \frac{1}{\sqrt{N}} \begin{pmatrix} a_k \\ b_k \end{pmatrix}, \quad (8)$$

where the forms of a_k and b_k depend on impurity position on the lattice, N is an integer representing the number of unit cells of the graphene lattice ($N \rightarrow \infty$). Eq. (6) can be rewritten in the matrix form

$$\Delta(z) = \frac{1}{N} \sum_k \begin{pmatrix} a_k^* & b_k^* \end{pmatrix} \cdot \begin{pmatrix} z & \pi_k \\ \pi_k^* & z \end{pmatrix}^{-1} \cdot \begin{pmatrix} a_k \\ b_k \end{pmatrix}. \quad (9)$$

We denote

$$M_k = \begin{pmatrix} z & \pi_k \\ \pi_k^* & z \end{pmatrix}^{-1}. \quad (10)$$

Difficulties arise when one attempts to calculate retarded function (by replacing z by $\omega + i0^+$) as he/she needs to treat of the simple poles in M_k properly in order to obtain Dirac delta functions in the hybridization spectrum $h(\omega) = -\frac{1}{\pi} \text{Im}\Delta(\omega + i0^+)$.

To treat the poles in Eq. (9), we separate simple poles into different terms and keep track of them during the calculations. First, we write M_k in the diagonal form

$$M_k = P_k \cdot D_k \cdot P_k^\dagger, \quad (11)$$

where D_k is diagonal matrix

$$D_k = \begin{pmatrix} \frac{1}{z - |\pi_k|} & 0 \\ 0 & \frac{1}{z + |\pi_k|} \end{pmatrix}, \quad (12)$$

and P_k is the transformation matrix

$$P_k = \frac{1}{\sqrt{2}} \begin{pmatrix} \pi_k & -\pi_k \\ |\pi_k| & |\pi_k| \end{pmatrix}. \quad (13)$$

We then obtain

$$\Delta(z) = \frac{1}{N} \sum_k \left[\frac{(|a_k|^2 + |b_k|^2)/2 + \text{Re}(\pi_k a_k^* b_k)/|\pi_k|}{z - |\pi_k|} + \frac{(|a_k|^2 + |b_k|^2)/2 - \text{Re}(\pi_k a_k^* b_k)/|\pi_k|}{z + |\pi_k|} \right]. \quad (14)$$

Thus in Eq. (14), we separate $\Delta(z)$ into two terms corresponding to two simple poles $z = \pm|\pi_k|$ as described above.

4. Results

Similar to the construction of H_{latt} , the hybridization part H_{hyb} is constructed using the tight-binding approach, where the hoppings of electrons between the impurity and nearby lattice sites are considered. Therefore $V_{k\alpha}$ is the Fourier transform of the real space tight-binding hybridization

$$V_{k\alpha} = \frac{1}{\sqrt{N}} \sum_R e^{-ik \cdot (R + \tau_\alpha - R_{imp})} V(R + \tau_\alpha, R_{imp}), \quad (15)$$

where R is the lattice vector (position vector of a unit cell), τ_α is the position vector of an atom belonging to sublattice α (A or B) in a unit cell, R_{imp} is the position of the impurity on the lattice, $V(R + \tau_\alpha, R_{imp})$ is the hopping of electrons between site $R + \tau_\alpha$ and the impurity. We note that all the vectors in Eq. (15) are assumed two-dimensional vectors. If the impurity is at a distance above the graphene sheet, without the loss of generality, we choose R_{imp} as the projection of the impurity vector to the lattice.

Normally, the dominant term of $V(R + \tau_\alpha, R_{imp})$ is the nearest-neighbor hybridization (in analogy to tight-binding electron hopping), which we denote as v_0 . The amplitudes of further

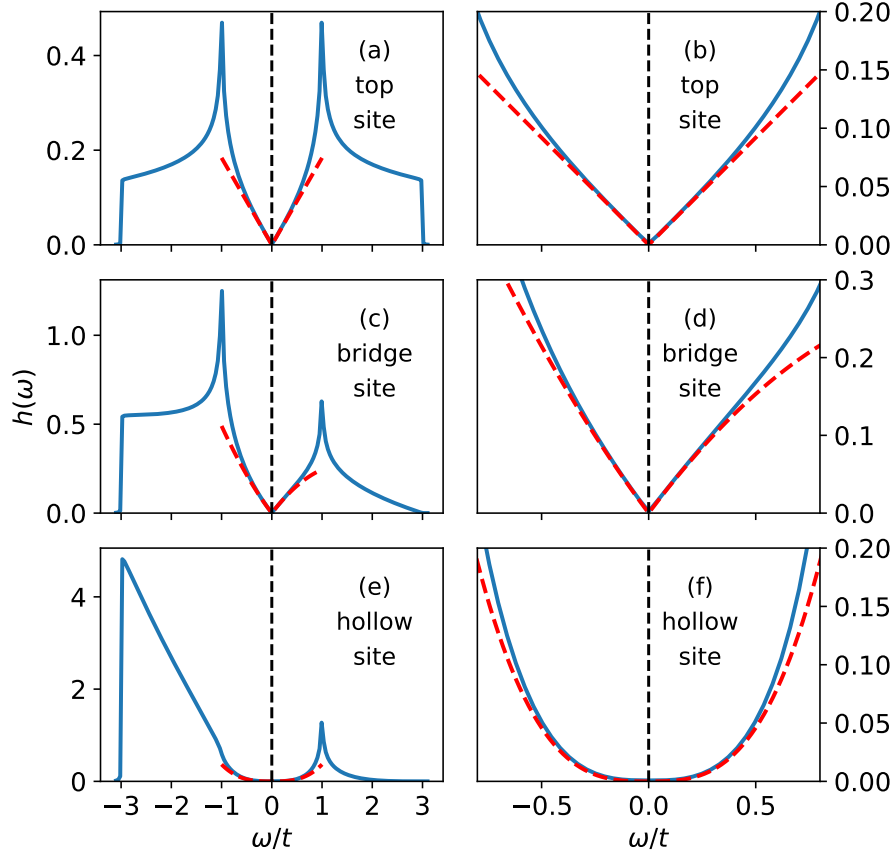


Fig. 2. The hybridization spectra $h(\omega)$ for different impurity positions. (a), (c), (e): The spectra $h(\omega)$ corresponding to impurity at the t site, b site and h site, respectively, for the whole active range ω from $-3t$ to $3t$. (b), (d), (f): The expanded view of $h(\omega)$ in panels (a), (c), (e), respectively, with ω in the range $[-0.8t, 0.8t]$. The vertical dashed line in each panel marks the Fermi level. The red dashed curves are $h(\omega)$ at low frequency plotted using the analytic formulas obtained in the main text.

hybridizations decrease exponentially with respect to the distance to the impurity. It is reasonable for low-energy physics problem such as the Kondo effect to consider only the nearest neighbor terms in Eq. (15)

$$V(R + \tau_\alpha, R_{imp}) = \begin{cases} v_0 & \text{at } \min |R + \tau_\alpha - R_{imp}|, \\ 0 & \text{otherwise.} \end{cases} \quad (16)$$

Even for the same v_0 , the number of nearest neighbor sites as well as the distance to the impurity changes depending on the position of the impurity. Thus, it is important to treat the hybridization function separately at each impurity position. In the following subsections, we present our derivation for the analytic form of the hybridization spectrum $h(\omega) = -\frac{1}{\pi} \text{Im} \Delta(\omega + i0^+)$ at low frequency for 3 common impurity positions on graphene lattice. The result for each position is justified by a plot comparing the numerical calculation of the spectrum (blue solid line) with the analytic curve

(red dashed line) in Figure 2. The numerical results of $h(\omega)$ are obtained by directly calculating Eq. (14), while the analytic results are derived separately for each case of impurity position. The validity of the analytic expressions is further analyzed and confirmed in Appendix 1

We also note that while knowing the stable position of the impurity is essential to interpret the Kondo physics in graphene, the ground-state position of the impurity depends very much on its chemical element. While alkali metals (Na, K ...) or alkaline earth metals (such as Ca) with only s electrons tend to stay at the hollow site due to their spherically-symmetric s orbital [5], elements without spherically-symmetric valence electrons such as boron is more likely located at the bridge or at the top site [30,31]. Transition metals, on the other hand, are more complicated due to their d valence electrons, the ground-state impurity position varies [6]. Thus determining precise position of impurity on the graphene lattice is still an open question, which is however beyond the scope of this paper.

4.1. At the t site

When the impurity is on top of a carbon atom in the graphene sheet, the impurity hybridizes directly with that atom underneath. Assuming the atom underneath belongs to the sublattice A , we obtain $a_k = v_0$ and $b_k = 0$. Replacing these a_k and b_k into Eq. (14), the hybridization function is directly proportional to the onsite Green function of the lattice

$$\Delta(z) = \frac{v_0^2}{2} \frac{1}{N} \sum_k \left(\frac{1}{z - |\pi_k|} + \frac{1}{z + |\pi_k|} \right). \quad (17)$$

Considering the retarded function ($z \rightarrow \omega + i0^+$), we have the hybridization spectrum

$$\begin{aligned} h(\omega) &= -\frac{1}{\pi} \text{Im} \Delta(\omega + i0^+) \\ &= \frac{v_0^2}{2} \frac{1}{N} \sum_k [\delta(\omega - |\pi_k|) + \delta(\omega + |\pi_k|)]. \end{aligned} \quad (18)$$

Thus the hybridization spectrum is exactly the DOS of graphene multiplied by a prefactor $\frac{v_0^2}{2}$

$$h(\omega) = \frac{v_0^2}{2} \nu(\omega). \quad (19)$$

Figure 2(a) shows the numerical calculation of $h(\omega)$ for impurity at the t site, which indeed exhibits the shape of graphene DOS where only the nearest neighbor hopping t is included.

We attempt to expand the hybridization spectrum to low energy in order to understand its behaviors and predict the solution of the impurity problem. It is well-known that around the valley K and K' of graphene [defined in Fig. 1(b)], the energy dispersion relation is linear with respect to the wave vector [4]. Thus if defining \vec{q} as the vector in the k space determining the distance from the valley K or K' ($\vec{k} = \vec{K} + \vec{q}$ or $\vec{k} = \vec{K}' + \vec{q}$, respectively) and the magnitude $q = |\vec{q}|$, for $q \ll |\vec{K}|$, the energy dispersion relation is [4]

$$\epsilon_k \approx \pm v_F q, \quad (20)$$

where $v_F = 3t/2$ is the Fermi velocity. The DOS of graphene around the Fermi level is contributed by energy dispersion around the two valleys

$$\begin{aligned}
 \nu(\omega) &= \frac{1}{N} \sum_{k \in BZ1} \delta(\omega - \epsilon_k) \\
 &= \int_{BZ1} \frac{d^2k}{A_{BZ1}} [\delta(\omega - |\pi_k|) + \delta(\omega + |\pi_k|)] \\
 &\approx \frac{2}{A_{BZ1}} \int_0^\infty q dq \int_0^{2\pi} d\phi \delta(\omega - v_F q) + \delta(\omega + v_F q) \\
 &= \frac{4\pi}{A_{BZ1}} \frac{|\omega|}{v_F^2},
 \end{aligned} \tag{21}$$

where A_{BZ1} is the area of the first Brillouin zone. The k -integral is conducted around the two valleys K and K' , where the polar coordinate $\vec{q} = (q, \phi)$ is in use. The factor of 2 corresponds to the two valleys. Let $A_c = (2\pi)^2/A_{BZ1}$ be the area of a unit cell of the lattice, we obtain from Eq. (21) the DOS around the Fermi level as [4]

$$\nu(\omega) = \frac{A_c}{\pi v_F} \frac{|\omega|}{v_F}. \tag{22}$$

Therefore, at the t site, the hybridization spectrum in proximity to the Fermi level reads

$$h(\omega) = \frac{v_0^2 A_c}{2\pi v_F} \left(\frac{|\omega|}{v_F} \right). \tag{23}$$

Fig. 2(b) confirms this linear behavior by comparing the numerically calculated $h(\omega)$ with the lines plotted using Eq. (23). Consequently, as the hybridization spectrum is exactly the same as the DOS of graphene (different by only a prefactor $\frac{v_0^2}{2}$), an s -wave single-orbital impurity on top of a carbon atom well represents the case of the pseudogap Kondo model at $r = 1$.

4.2. At the b site

When the impurity is away from the t site, the situation changes. At a glance, the hybridization spectrum is no longer symmetric around the Fermi level [see Figs. 2(c), (e)] due to the hybridization of the impurity with sites of both sublattices [24]. When the impurity is at the b site [Figs. 2(c)], the hybridization spectrum for $\omega < 0$ is slightly larger than that for $\omega > 0$, which does not exist in the conventional pseudogap Kondo model. Nevertheless, the behavior of the hybridization spectrum at low energy is more important, which is fully derived in this subsection.

At the b site, using Eqs. (15) and (16), the hybridization strength has the form

$$a_k = \frac{v_0}{\exp\left(\frac{ik\tau_B}{2}\right)}, \tag{24}$$

$$b_k = a_k^* = \frac{v_0}{\exp\left(\frac{-ik\tau_B}{2}\right)}. \tag{25}$$

As a result, the hybridization function is

$$\begin{aligned}\Delta(z) &= \frac{v_0^2}{N} \sum_k \left[\frac{v_0^2 + \text{Re}(\alpha_k a_k^* b_k)}{z - |\pi_k|} + \frac{v_0^2 - \text{Re}(\alpha_k a_k^* b_k)}{z + |\pi_k|} \right] \\ &= \frac{v_0^2}{N} \sum_k \left[\frac{1}{z - |\pi_k|} + \frac{1}{z + |\pi_k|} \right] + \frac{1}{N} \sum_k \left[\frac{\text{Re}(\alpha_k a_k^* b_k)}{z - |\pi_k|} - \frac{\text{Re}(\alpha_k a_k^* b_k)}{z + |\pi_k|} \right]\end{aligned}\quad (26)$$

After replacing z by $\omega + i0^+$ and calculating the imaginary part of $\Delta(z)$, the hybridization spectrum $h(\omega)$ composes of two terms: the first summation in Eq. (26) turns into the DOS of graphene, while the second summation can be obtained analytically at low frequency

$$h(\omega) = v_0^2 \nu(\omega) + \int \frac{d^2k}{A_{BZ1}} [\text{Re}(\alpha_k a_k^* b_k) \delta(\omega - |\pi_k|) - \text{Re}(\alpha_k a_k^* b_k) \delta(\omega + |\pi_k|)]. \quad (27)$$

In proximity to one of the two valleys such as K , we have $\vec{k} = \vec{K} + \vec{q}$. Again we use the polar coordinate system $\vec{q} = (q, \phi)$ and conduct expansion over $q = |\vec{q}|$ to the lowest order for the spectrum around the Fermi level. At the lowest order of q , $|\pi_k| = v_F q + O(q^3)$, the Dirac delta functions in Eq. (27) do not depend on ϕ , allowing us to integrate only the numerator $\text{Re}(\alpha_k a_k^* b_k)$ over the polar angle ϕ . The result is greatly simplified

$$\begin{aligned}\int_0^{2\pi} \text{Re}(\alpha_k a_k^* b_k) d\phi &= \int_0^{2\pi} \text{Re} \frac{v_0^2 e^{-ik\tau_B} \pi_k}{|\pi_k|} d\phi \\ &= v_0^2 (-\pi q + O(q^3)).\end{aligned}\quad (28)$$

Replacing $|\pi_k|$ by its first order term into Eq. (27), the hybridization spectrum for ω around the Fermi level is

$$h(\omega) = v_0^2 \nu(\omega) + v_0^2 \frac{2\pi}{A_{BZ1}} \int_0^\infty dq q^2 [\delta(\omega + v_F q) - \delta(\omega - v_F q)]. \quad (29)$$

As we focus on the region around the Fermi level, the integrating region is composed of the neighborhoods of the two valleys K and K' , resulting a factor of 2 in the above formula. Given that $A_{BZ1} = (2\pi)^2/A_c$, we have

$$h(\omega) = v_0^2 \nu(\omega) + \frac{v_0^2 A_c}{2\pi} \frac{-\omega^2}{v_F^3} \text{sgn}(\omega). \quad (30)$$

From Eq. (22), at the lowest ω order, $\nu(\omega) = \frac{A_c}{\pi v_F} \frac{|\omega|}{v_F}$, the final form of $h(\omega)$ up to the second order of ω is

$$h(\omega) = \frac{v_0^2 A_c}{\pi v_F} \left(\frac{|\omega|}{v_F} - \frac{1}{2} \frac{\omega^2}{v_F^2} \text{sgn}(\omega) \right). \quad (31)$$

In Eq. (31), one can see that the lowest order of ω exhibits $r = 1$ -pseudogap Kondo model, asymmetric contributions start at the second order of ω , which increases the spectrum for $\omega < 0$ and decreases it for $\omega > 0$, consistent with Fig. 2(c). The expanded view of $h(\omega)$ in Fig. 2(d), which plots the numerical $h(\omega)$ in comparison with the curve of Eq. (31), justifies the correctness of our calculation. The low-energy characteristic of the Kondo effect means that the dominant term in Eq. (31) is indeed the first order term in ω , which does not exhibit the asymmetry in $h(\omega)$. Therefore, for impurities at the b site, the asymmetry in the hybridization spectrum does not affect

much the pseudogap Kondo effect, explaining why the phase transition for impurity at this position is not significantly different from that at the t site, as seen elsewhere [24].

4.3. At the h site

Lastly, when the impurity is placed at the h site of the graphene lattice, there are six nearest neighbor sites located at each vertex of the hexagon to which the impurity belongs. Given that there are only two nearest neighbor sites for the impurity at the b site and one for the impurity at the t site, there can be a significant change in the hybridization spectrum when the impurity is at the h site. In other words, the coordination number of the impurity may play an important role in the hybridization function.

Indeed, Fig. 2(e) shows significant differences in $h(\omega)$ for the h -site case as compared with the t - and b -site cases. In the following, we will present our analytic calculation and show that the lowest order ω term of $h(\omega)$ for impurity at the h site is no longer the first order and that the hybridization weight around the Fermi level is strongly diminished.

Employing Eq. (15), the hybridization strength $V_{k\alpha}$ has the components

$$a_k = v_0 \pi_k^*, \quad (32)$$

$$b_k = v_0 \pi_k, \quad (33)$$

similar to the off-diagonal elements in the tight-binding matrix in Eq. (3) (where π_k is from Eq. (4)). Replacing these a_k and b_k into Eq. (6), the form of the hybridization function becomes

$$\Delta(z) = \frac{v_0^2}{N} \sum_k \left[\frac{|\pi_k|^2 + \text{Re}(\pi_k^3/|\pi_k|)}{z - |\pi_k|} + \frac{|\pi_k|^2 - \text{Re}(\pi_k^3/|\pi_k|)}{z + |\pi_k|} \right]. \quad (34)$$

Again, when focusing on the neighborhood of the Fermi level, the same procedure as those in the calculations for the t site and b site case is applied. In the k -integral, we only concentrate on the region around the valleys K and K' . Again, the variable for integration is changed from k to $q = k - K$ (or $q = k - K'$)

$$\Delta(z) = \frac{v_0^2}{A_{BZ1}} \int_0^\infty q dq \int_0^{2\pi} d\phi \left[\frac{|\pi_k|^2 + \text{Re}(\pi_k^3/|\pi_k|)}{z - v_F q} + \frac{|\pi_k|^2 - \text{Re}(\pi_k^3/|\pi_k|)}{z + v_F q} \right]. \quad (35)$$

In Eq. (35), we can integrate first the variable ϕ with the integrands being the numerators in the expression.

$$K_q = \int_0^{2\pi} \left[|\pi_{K+q}|^2 \pm \text{Re} \frac{\pi_{K+q}^3}{|\pi_{K+q}|} \right] d\phi. \quad (36)$$

At small q , K_q exhibits an interestingly simple form

$$K_q = \frac{9\pi q^2}{2} + O(q^3). \quad (37)$$

Substitute K_q into Eq. (35) and put in a factor of 2 for the contributions of two valleys K and K'

$$\Delta(z) = \frac{2v_0^2}{A_{BZ1}} \int_0^\infty dq \frac{9\pi q^3}{2} \left(\frac{1}{z - v_F q} + \frac{1}{z + v_F q} \right). \quad (38)$$

We change $z \rightarrow \omega + i0^+$ and calculate the imaginary part for the hybridization spectrum $h(\omega)$ (using $A_c = (2\pi)^2/A_{BZ1}$)

$$h(\omega) = v_0^2 \frac{9A_c}{4\pi} \int_0^\infty dq q^3 [\delta(\omega - v_F q) + \delta(\omega + v_F q)]. \quad (39)$$

This integral is easily calculated, leading to the final form of the hybridization spectrum at the lowest order of ω as

$$h(\omega) = v_0^2 \frac{9A_c}{4\pi v_F} \left(\frac{|\omega|}{v_F} \right)^3. \quad (40)$$

It is interesting that for the case of the impurity at the h site, $|\omega|^3$ is the lowest order, different from the other two cases where the first order of ω is the lowest one. Our comparison between numerical calculation and Eq. (40) in Fig. 2(f) confirms the validity of the analytic calculation of $h(\omega)$ at small ω . Furthermore, Appendix 1 analyzes this case in detail, showing that numerical calculations indeed converge to Eq. (40).

The h -site case therefore exhibits a different kind of pseudogap Kondo problem with $r = 3$ (parameter r is mentioned in Sec. 1). As a result, the $r = 3$ -pseudogap model has different physics from the $r = 1$ case. When fully considering the correlation effect, $r = 1$ model exhibits the behaviors of the “upper critical dimension” in analogy to the critical field theory, in which there is logarithmic correction to many kinds of scaling laws [32] and nontrivial renormalization group (RG) fixed points disappear above this limit [33, 34]. Above this “upper critical dimension”, the full solution of the $r = 3$ case is expected to be obtained with an appropriate mean-field approach or perturbative RG calculation.

Furthermore, when comparing Eq. (40) with the hybridization spectra of other cases at low energy, assuming the same v_0 , the prefactors $\sim v_0^2 \frac{A_c}{\pi v_F}$ are of the same order, while ω can be written in a dimensionless variable $\frac{\omega}{v_F}$. As $v_F = \frac{3t}{2}$ is of order t , for ω near the Fermi level ($\omega \ll v_F$), the spectral weight of $h(\omega)$ at the h site is much smaller than that of the other two cases for a wide range of ω (from $-0.5t$ to $0.5t$). In practice, this depletion in the spectrum leads to extreme experimental conditions in order to observe the Kondo screening phase. Realization of the pseudogap Kondo effect on graphene lattice, especially for impurity at the h site, thus can be a nontrivial task.

5. Conclusions

In this work, we have studied the hybridization function for the pseudogap Anderson model on the graphene lattice, where the DOS around the Fermi level is $\sim |\omega|^r$ ($r = 1$ for graphene). We did not fully solve the pseudogap impurity problem, instead, we introduced an approach for deriving analytical formulas for the hybridization spectrum at low-energy for different impurity positions, which are crucial for predicting the solution of the impurity problem.

We have derived analytic expressions of the hybridization spectrum at low frequency for three impurity positions and summarized in Table 1. These expressions show that it is important to consider the lattice effects even for low-energy physics such as the Kondo effect. In our case, depending on the position of the impurity on the lattice, the hybridization spectrum can be changed drastically from the $|\omega|$ to $|\omega|^3$ behavior as the impurity changes from the top or bridge site to the hollow site on the graphene lattice. It implies that the nature of the pseudogap Kondo physics is significantly affected. The pseudogap problem with $|\omega|$ behavior represents the “upper critical

Table 1. Summary of the hybridization spectrum $h(\omega) = -\frac{1}{\pi}\text{Im}\Delta(\omega + i0+)$ at the lowest order of $|\omega|/v_F$ for three cases of impurity located at t , b and h positions. $A_c = \frac{3\sqrt{3}}{2}$ is the area of the unit cell of the graphene lattice, $v_F = \frac{3t}{2}$ is the Fermi velocity.

Spectrum	t site	b site	h site
$h(\omega)$	$\frac{v_0^2 A_c}{2\pi v_F} \left(\frac{ \omega }{v_F} \right)$	$\frac{v_0^2 A_c}{\pi v_F} \left(\frac{ \omega }{v_F} \right)$	$\frac{9v_0^2 A_c}{4\pi v_F} \left(\frac{ \omega }{v_F} \right)^3$

dimension" limit in analogy to that in the critical field theory, while for $|\omega|^3$ behavior, quantum fluctuations are diminished, the impurity problem might be treated by an appropriate mean-field approach. More importantly, from experimental aspects, it suggests that one pay more attention to the impurity position on the lattice when conducting experiments to study the Kondo effect. The strong dependence of the hybridization function on the impurity position exposes difficulties for the observation of pseudogap Kondo effect on graphene. In particular, when the impurity is at the hollow site, the hybridization spectrum is depleted around the Fermi level, thus it requires extreme conditions such as very small temperature, parameter fine-tuning and high-resolution spectral measurement techniques, etc. to observe the Kondo effect. Because it is not easy to pin down the position of the impurity, it results in an overall difficulty that hinders experimental realization of the pseudogap Kondo effect on graphene.

This calculation approach is simple yet efficient for obtaining analytical form of the input hybridization function or even bare Green function, which is important for determining and classifying the pseudogap Kondo problem under investigation. It can be applied to more complicated system, for example, instead of the s -wave impurity, one can study the hybridization for a d -wave or f -wave multi-orbital impurity, which is more realistic for experiments with transition metal or rare-earth adatoms. The low-frequency hybridization function can thus be obtained for each kind of d or f orbital. We believe that, following this direction, one can have a qualitative picture of more complicated Kondo effects, allowing for further understanding of correlated adatoms on graphene.

Acknowledgements

This research is funded by Vietnam National Foundation for Science and Technology Development (NAFOSTED) under grant number 103.02-2021.95.

Authors contributions

Hoa T. M. Nghiem: Visualization, Investigation. Tien-Lam Pham: Validation, Writing - Review & Editing. Ngoc-Linh Nguyen: Validation, Writing - Review & Editing. Hung T. Dang: Methodology, Writing - Original Draft.

Conflict of interest

The authors declare that they have no competing financial interests.

References

- [1] K. S. Novoselov *et al.*, *Electric field effect in atomically thin carbon films*, *Science* **306** (2004) 666.
- [2] Y. Zhang, Y.-W. Tan, H. L. Stormer and P. Kim, *Experimental observation of the quantum hall effect and berry's phase in graphene*, *Nature* **438** (2005) 201.
- [3] K. S. Novoselov *et al.*, *Two-dimensional gas of massless dirac fermions in graphene*, *nature* **438** (2005) 197.
- [4] A. H. Castro Neto, F. Guinea, N. M. R. Peres, K. S. Novoselov and A. K. Geim, *The electronic properties of graphene*, *Rev. Mod. Phys.* **81** (2009) 109.
- [5] K. T. Chan, J. B. Neaton and M. L. Cohen, *First-principles study of metal adatom adsorption on graphene*, *Phys. Rev. B* **77** (2008) 235430.
- [6] M. Manadé, F. Viñes and F. Illas, *Transition metal adatoms on graphene: A systematic density functional study*, *Carbon* **95** (2015) 525.
- [7] G. Fiori *et al.*, *Electronics based on two-dimensional materials*, *Nat. Nanotechnol.* **9** (2014) 768.
- [8] F. Ellinger, C. Franchini and V. Bellini, *Magnetic 3d adatoms on free-standing and ni(111)-supported graphene*, *Phys. Rev. Mater.* **5** (2021) 014406.
- [9] H.-Y. Zhuo *et al.*, *Theoretical understandings of graphene-based metal single-atom catalysts: Stability and catalytic performance*, *Chem. Rev.* **120** (2020) 12315.
- [10] D. Marchiani *et al.*, *Tuning the electronic response of metallic graphene by potassium doping*, *Nano Lett.* **23** (2023) 170.
- [11] P. T. Araujo, M. Terrones and M. S. Dresselhaus, *Defects and impurities in graphene-like materials*, *Mater. Today* **15** (2012) 98.
- [12] N. Dimakis *et al.*, *Density functional theory calculations on alkali and the alkaline ca atoms adsorbed on graphene monolayers*, *Appl. Surf. Sci.* **413** (2017) 197.
- [13] T. O. Wehling, A. V. Balatsky, M. I. Katsnelson, A. I. Lichtenstein and A. Rosch, *Orbitally controlled kondo effect of co adatoms on graphene*, *Phys. Rev. B* **81** (2010) 115427.
- [14] J. Ren *et al.*, *Kondo effect of cobalt adatoms on a graphene monolayer controlled by substrate-induced ripples*, *Nano Letters* **14** (2014) 4011 [<https://doi.org/10.1021/nl501425n>].
- [15] V. W. Brar *et al.*, *Gate-controlled ionization and screening of cobalt adatoms on a graphene surface*, *Nature Physics* **7** (2011) 43.
- [16] L. Fritz and M. Vojta, *The physics of kondo impurities in graphene*, *Reports on Progress in Physics* **76** (2013) 032501.
- [17] A. C. Hewson, *The Kondo problem to heavy fermions*, vol. 2. Cambridge university press, 1997.
- [18] D. Withoff and E. Fradkin, *Phase transitions in gapless fermi systems with magnetic impurities*, *Phys. Rev. Lett.* **64** (1990) 1835.
- [19] R. Bulla, T. Pruschke and A. C. Hewson, *Anderson impurity in pseudo-gap fermi systems*, *J. Phys. Condens. Matter* **9** (1997) 10463.
- [20] C. Gonzalez-Buxton and K. Ingersent, *Renormalization-group study of anderson and kondo impurities in gapless fermi systems*, *Phys. Rev. B* **57** (1998) 14254.
- [21] J. H. Pixley, S. Kirchner, K. Ingersent and Q. Si, *Kondo destruction and valence fluctuations in an anderson model*, *Phys. Rev. Lett.* **109** (2012) 086403.
- [22] P. Gegenwart, Q. Si and F. Steglich, *Quantum criticality in heavy-fermion metals*, *Nat. Phys.* **4** (2008) 186.
- [23] P. W. Anderson, *Localized magnetic states in metals*, *Phys. Rev.* **124** (1961) 41.
- [24] H. T. Dang and H. T. M. Nghiem, *Phase diagram of a pseudogap anderson model with application to graphene*, arXiv:2107.09854 [cond-mat.str-el] (2021) [[2107.09854](https://arxiv.org/abs/2107.09854)].
- [25] A. Georges, L. d. Medici and J. Mravlje, *Strong correlations from hund's coupling*, *Annual Review of Condensed Matter Physics* **4** (2013) 137.
- [26] A. Georges, G. Kotliar, W. Krauth and M. J. Rozenberg, *Dynamical mean-field theory of strongly correlated fermion systems and the limit of infinite dimensions*, *Rev. Mod. Phys.* **68** (1996) 13.
- [27] J. W. Negele and H. Orland, *Quantum many-particle systems*. CRC Press, 2018.
- [28] E. Gull *et al.*, *Continuous-time monte carlo methods for quantum impurity models*, *Rev. Mod. Phys.* **83** (2011) 349.

- [29] A. A. Abrikosov, L. P. Gorkov and I. E. Dzyaloshinski, *Methods of quantum field theory in statistical physics*. Courier Corporation, 2012.
- [30] S. Jubin, A. Rau, Y. Barsukov, S. Ethier and I. Kaganovich, *Boron adatom adsorption on graphene: A case study in computational chemistry methods for surface interactions*, *Front. Phys.* **10** (2022).
- [31] R. B. Pontes, A. Fazio and G. M. Dalpian, *Barrier-free substitutional doping of graphene sheets with boron atoms: Ab initio calculations*, *Phys. Rev. B* **79** (2009) 033412.
- [32] C. R. Cassanello and E. Fradkin, *Kondo effect in flux phases*, *Phys. Rev. B* **53** (1996) 15079.
- [33] L. Fritz and M. Vojta, *Phase transitions in the pseudogap anderson and kondo models: Critical dimensions, renormalization group, and local-moment criticality*, *Phys. Rev. B* **70** (2004) 214427.
- [34] M. Vojta and L. Fritz, *Upper critical dimension in a quantum impurity model: Critical theory of the asymmetric pseudogap kondo problem*, *Phys. Rev. B* **70** (2004) 094502.
- [35] N. W. Ashcroft and N. D. Mermin, *Solid State Phys.* Holt-Saunders, 1976.

Appendix 1: Convergence of the numerical solutions

Figure 2 is our main figure, which confirms the correctness of the analytic expressions in the main text by directly comparing them with numerical calculations of the hybridization spectra. Our numerical solutions contain an approximation because of a broadening η introduced to approximate the Dirac delta function by a Lorentzian, which causes a systematic error. This η parameter is inserted naturally during the analytical continuation process (the general frequency z in Eq. (6) is replaced by $\omega + i\eta$). The numerical exact solution could be obtained in the limit $\eta \rightarrow 0^+$. However it is computationally not feasible as the computational cost increases rapidly to infinity as $\eta \rightarrow 0$. In this appendix, we carry out the η -scaling analysis to show that our numerical solutions approach the analytic results.

We focus on the case of the impurity at the h site as the difference between the analytic formula [Eq. (40)] and the numerical solution in this case is the largest. Figure 3(a) shows the difference between numerical calculations and the analytic results $|h(\omega) - h_{\text{analytic}}(\omega)|$ in the low-frequency region. The decrease of the difference in direct proportion with the decrease of η at $\omega = 0$ suggests the linear relation between this difference and η . We verify this relation in Fig. 3(b) by linearly fitting the hybridization spectrum at $\omega = 0$ with respect to η . Fig. 3(b) exhibits a perfect linear relation between $h(\omega = 0)$ and η . Extrapolation to $\eta = 0$ results in $h(\omega = 0) = 5(3) \times 10^{-5}$, which almost vanishes, consistent with Eq. (40) at $\omega = 0$. It allows us to estimate $h(\omega)$ at $\eta \rightarrow 0$ limit by linearly extrapolating $h(\omega)$ for a wide range of ω . The extrapolated $h(\omega)$ is nearly the same as the analytic form in the range $-0.2t < \omega < 0.2t$. (For larger frequency, it requires higher order terms of ω for better accuracy.)

The peculiar point is at $\omega = t$, which is the frequency for the van Hove singularity in $h(\omega)$, where the extrapolation does not work. As we plot in Fig. 3(c), the linear relation between $h(\omega = t)$ and $\log \eta$ means that $h(\omega = t)$ diverges exponentially with respect to $1/\eta$, which is indeed a characteristic of the van Hove singularity [35]. Therefore, linear extrapolation near the van Hove singularity requires much smaller η to maintain the same quality. However, as we focus on low frequency, the van Hove point is beyond the range of interest and does not severely affect the convergence of $h(\omega)$ to the analytic formula.

Therefore, this appendix shows that, for impurity at the h site, the spectral function behaves in a well-known manner with respect to η and that it indeed converges to the analytic form of $h(\omega)$ at low frequency. Other cases of impurity at the t and b sites are expected to behave in a similar manner. Thus it justifies the validity of our analytic derivation of $h(\omega)$ at low frequency.

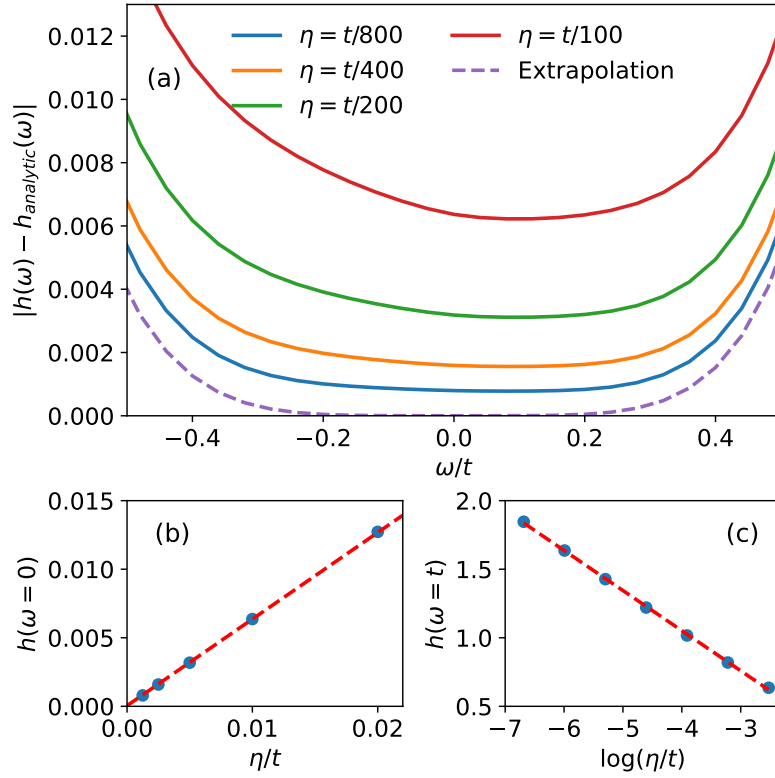


Fig. 3. (a) Plot of the difference $|h(\omega) - h_{analytic}(\omega)|$ between the analytic formula [Eq. (40)] and the numerical calculation of $h(\omega)$ for the case of the impurity at the h site. The broadening η decreases corresponding to curves appearing in the top-down direction. The dashed curve is the linearly extrapolated $h(\omega)$ as $\eta \rightarrow 0$. (b) Linear fit (red line) of the hybridization spectral value at $\omega = 0$ with respect to η . (c) Linear fit (red line) of the hybridization spectral value at $\omega = t$ with respect to $\log(\eta/t)$.